NASA/TM—2011-217124

Computational Assessment of the Aerodynamic Performance of a Variable-Speed Power Turbine for Large Civil Tilt-Rotor Application

Gerard E. Welch
Glenn Research Center, Cleveland, Ohio

November 2011

NASA STI Program . . . in Profile

Since its founding, NASA has been dedicated to the advancement of aeronautics and space science. The NASA Scientific and Technical Information (STI) program plays a key part in helping NASA maintain this important role.

The NASA STI Program operates under the auspices of the Agency Chief Information Officer. It collects, organizes, provides for archiving, and disseminates NASA's STI. The NASA STI program provides access to the NASA Aeronautics and Space Database and its public interface, the NASA Technical Reports Server, thus providing one of the largest collections of aeronautical and space science STI in the world. Results are published in both non-NASA channels and by NASA in the NASA STI Report Series, which includes the following report types:

- TECHNICAL PUBLICATION. Reports of completed research or a major significant phase of research that present the results of NASA programs and include extensive data or theoretical analysis. Includes compilations of significant scientific and technical data and information deemed to be of continuing reference value. NASA counterpart of peer-reviewed formal professional papers but has less stringent limitations on manuscript length and extent of graphic presentations.

- TECHNICAL MEMORANDUM. Scientific and technical findings that are preliminary or of specialized interest, e.g., quick release reports, working papers, and bibliographies that contain minimal annotation. Does not contain extensive analysis.

- CONTRACTOR REPORT. Scientific and technical findings by NASA-sponsored contractors and grantees.

- CONFERENCE PUBLICATION. Collected papers from scientific and technical conferences, symposia, seminars, or other meetings sponsored or cosponsored by NASA.

- SPECIAL PUBLICATION. Scientific, technical, or historical information from NASA programs, projects, and missions, often concerned with subjects having substantial public interest.

- TECHNICAL TRANSLATION. English-language translations of foreign scientific and technical material pertinent to NASA's mission.

Specialized services also include creating custom thesauri, building customized databases, organizing and publishing research results.

For more information about the NASA STI program, see the following:

- Access the NASA STI program home page at *http://www.sti.nasa.gov*

- E-mail your question via the Internet to *help@sti.nasa.gov*

- Fax your question to the NASA STI Help Desk at 443–757–5803

- Telephone the NASA STI Help Desk at 443–757–5802

- Write to:
  NASA Center for AeroSpace Information (CASI)
  7115 Standard Drive
  Hanover, MD 21076–1320

NASA/TM—2011-217124

Computational Assessment of the Aerodynamic Performance of a Variable-Speed Power Turbine for Large Civil Tilt-Rotor Application

Gerard E. Welch
Glenn Research Center, Cleveland, Ohio

Prepared for the
67th Annual Forum and Technology Display (Forum 67)
sponsored by the American Helicopter Society
Virginia Beach, Virginia, May 3–5, 2011

National Aeronautics and
Space Administration

Glenn Research Center
Cleveland, Ohio 44135

November 2011

Acknowledgments

The author is grateful to Dr. Rodrick V. Chima for his expert assistance with his RANS tools and to Dr. John P. Clark (AFRL) for facilitating use of the AFRL Turbine Design and Analysis System (TDAAS) at NASA. This work was funded by the NASA Fundamental Aeronautics program, Subsonic Rotary Wing project.

This report contains preliminary findings, subject to revision as analysis proceeds.

This work was sponsored by the Fundamental Aeronautics Program at the NASA Glenn Research Center.

Level of Review: This material has been technically reviewed by technical management.

Available from

NASA Center for Aerospace Information
7115 Standard Drive
Hanover, MD 21076–1320

National Technical Information Service
5301 Shawnee Road
Alexandria, VA 22312

Available electronically at http://www.sti.nasa.gov

Computational Assessment of the Aerodynamic Performance of a Variable-Speed Power Turbine for Large Civil Tilt-Rotor Application

Gerard E. Welch
National Aeronautics and Space Administration
Glenn Research Center
Cleveland, Ohio 44135

Abstract

The main rotors of the NASA Large Civil Tilt-Rotor notional vehicle operate over a wide speed-range, from 100% at take-off to 54% at cruise. The variable-speed power turbine offers one approach by which to effect this speed variation. Key aero-challenges include high work factors at cruise and wide (40 to 60°) incidence variations in blade and vane rows over the speed range. The turbine design approach must optimize cruise efficiency and minimize off-design penalties at take-off. The accuracy of the off-design incidence loss model is therefore critical to the turbine design. In this effort, 3-D computational analyses are used to assess the variation of turbine efficiency with speed change. The conceptual design of a 4-stage variable-speed power turbine for the Large Civil Tilt-Rotor application is first established at the meanline level. The design of 2-D airfoil sections and resulting 3-D blade and vane rows is documented. Three-dimensional Reynolds Averaged Navier-Stokes computations are used to assess the design and off-design performance of an embedded 1.5-stage portion—Rotor 1, Stator 2, and Rotor 2—of the turbine. The 3-D computational results yield the same efficiency versus speed trends predicted by meanline analyses, supporting the design choice to execute the turbine design at the cruise operating speed.

Nomenclature

AN^2	product of annulus area and shaft-speed squared
c_x	axial chord
h_0, h	total and static specific enthalpy
i, i_{opt}	incidence, incidence at minimum loss
N	power-turbine shaft speed
N^*	$N/N_{100\%}$, fraction of 100% speed
PR_{TT}	overall total-pressure ratio
p_0, p	total and static pressure
Re_{cx}	Reynolds number based on axial chord
s	blade pitch, or specific entropy
T_0	total temperature
TR_{TT}	overall total-temperature ratio
Tu	turbulence intensity
$\underline{u}$	(u_x, u_θ, u_r), absolute velocity
U	rotor speed at pitchline
Y	$\frac{p_{0,1}-p_{0,2}}{p_{0,1}-p_2}$, loss coefficient
Z	$\frac{s}{c_x}\frac{\rho u_x(u_{\theta,1}-u_{\theta,2})}{p_{0,r,1}-p_2}$, Zweifel loading parameter
W	weight flow
α, β	absolute and relative flow angles
η_{TT}	adiabatic efficiency (total-to-total)
κ	turbulent kinetic energy
ρ	density
ψ	$\Delta h_0/U^2$, work factor
ϕ	u_x/U, flow coefficient
ω	vorticity

Subscripts

c	corrected to standard day
1, 2	Blade-row inlet, blade-row exit
4.5	power turbine inlet
r	rotor (blade), or relative condition

Introduction

A key challenge of the NASA Large Civil Tilt-Rotor (LCTR) mission is the required variation of main rotor tip-speed from 650 ft/s (100%) at take-off to 350 ft/s (54%) at cruise (Ref. 1). The wide speed variation can be accomplished by using a multi-speed transmission with a fixed-speed power turbine. Alternatively, the speed change can be effected by varying the speed of the power turbine rather than the transmission gear-ratio. The variable-speed power-turbine (VSPT) approach is used in the V-22, in which the output speed of the AE1107 engine varies speed in the range $80\% < N/N_{100\%} < 100\%$ (Ref. 2). The present study was focused on the VSPT approach to meeting the speed range requirement of the LCTR mission.

Results from NASA engine cycle studies (Ref. 3) were used to determine that LCTR power-turbine enthalpy extraction levels at take-off and cruise are nearly equal; therefore, the work factor, $\Delta h_0/U^2$, at cruise (54% N^*) is about 3.5 times that at take-off (100% N^*). The high work factors at cruise, speed-change requirement, and 28-kft altitude operation lead to significant aero-challenges (Ref. 4): (1) attainment of high efficiency at high work factor; (2) management of large (40 to

60°) incidence swings in all embedded vane/blade rows, and (3) operation at low (60 to 100 k) Reynolds number. The present study is focused on performance levels at design-point (28 kft cruise, 54% N^*) and off-design (2 kft take-off, 100% N^*), and in particular the variation in VSPT performance with shaft-speed change.

A conceptual aero-design approach for the VSPT of the LCTR application was outlined earlier (Ref. 4). The design air-angles of a 4-stage VSPT were set at the cruise operating condition (54% N^*) where Reynolds numbers were lowest and work factors ($\Delta h_0/U^2$) were highest. The impact of design point work factor on efficiency is documented in Figure 1. In addition to illustrating the decrease in design-point efficiency with work factor, the impact of operation at high (40 to 60°) negative incidence at the 100% speed take-off condition is shown as well. The meanline results—for example, compare the two green triangles of the present study—indicate that efficiency at the off-design take-off point is higher than at the cruise design-point. At off-design, although the air-angles are far from design, the turbine is lightly loaded (aerodynamically) and blade-row turning is low. The stage efficiency potential at the low work factor is high enough that, even with high incidence-induced loss production, the off-design efficiency exceeds that at design. The accuracy of this predicted trend depends strongly on the incidence correlation of the meanline system.

In an earlier study (Ref. 4), 2-D CFD analyses (Fig. 2(a)) were used to assess the range of useful incidence as a function of Reynolds number for the relevant LPT mid-span section of Clark et al. (Ref. 11). The 100% N^* operating condition had 50° of negative incidence, leading to a separated region in the cove on the blade pressure-side (Fig. 2(a)). In spite of the pressure-side separation, the profile loss at –50°. incidence was quite acceptable. In the same study (Ref. 4), the loss buckets in Figure 2(a) were shown to collapse on the standard Ainley-Mathieson incidence-loss correlation (Ref. 12). Thus, the efficiency versus operating speed trend of the meanline was substantiated by the loss buckets of the 2-D analysis. The 2-D and meanline analyses omit loss mechanisms and flow structures associated with 3-D aerodynamics and acceleration fields due to rotation. Considering Figure 2(b), for example, it is clear that the benign cove separation of the 2-D analysis is associated with a tornado like structure which transports low momentum flow radially outward toward the casing. The reset of the spanwise flow by secondary flows and radial transport is of particular concern in blade rows with high aerodynamic loading levels and turning. The present work was motivated by the need to verify, at the 3-D level, the loss versus incidence correlation of vane and blade (rotating) rows.

The key objective of the present effort was to conduct 3-D aero-design and analysis of a relevant stage of the VSPT turbine at a level sufficient to verify that the design (54% N^*) and off-design (100% N^*) performance of 3-D computational results is consistent with the meanline design/analysis used in the conceptual design of the VSPT for the LCTR. The paper is organized as follows: The aerodynamic design methodology, including meanline analysis used to design the 4-stage VSPT and 3-D design used to design incidence-tolerant blading, is first provided. Computational analysis of a selected three blade-row embedded 1.5-stage at design and off-design conditions is then provided to gauge performance potential and variation with shaft speed. Finally, conclusions from the present study are provided.

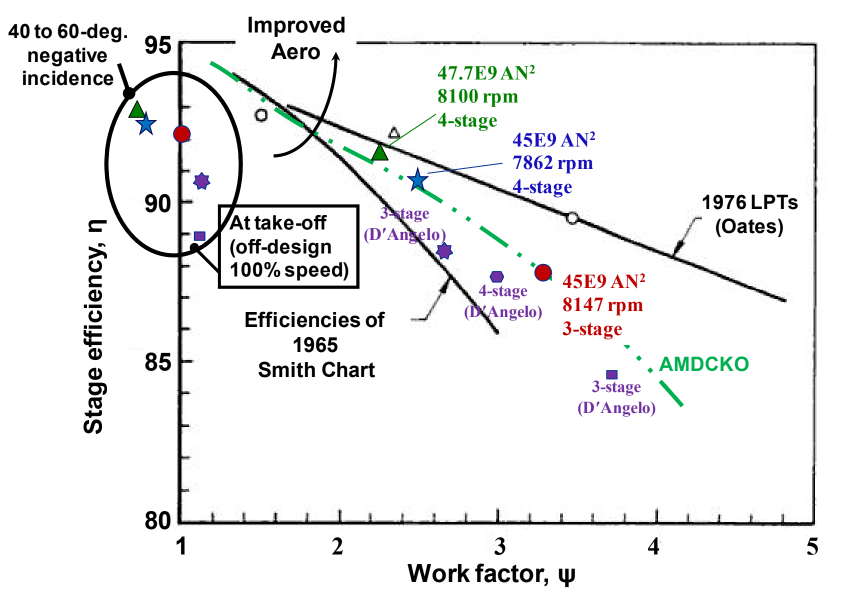

Figure 1.—Modified Smith chart showing design-point efficiency as a function of work factors for 3- and 4-stage VSPT meanline designs by Welch (Ref. 4) and D'Angelo (Ref. 5), compared with open literature (AMDCKO) (Refs. 6 to 8) meanline performance, Smith data (Ref. 9) and LPT turbine data (Ref. 10).

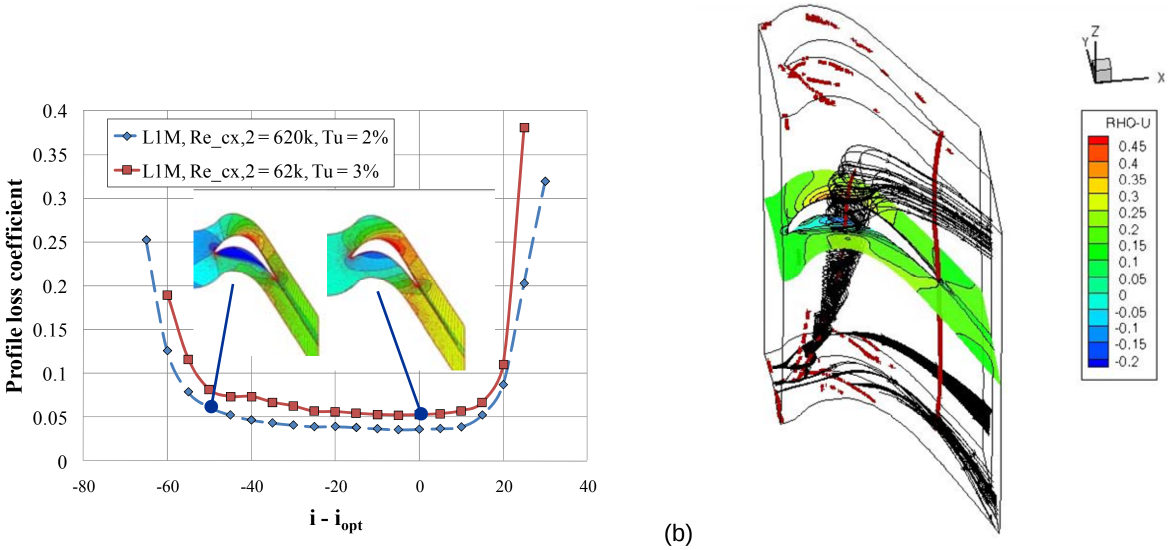

(a) (b)

Figure 2.—Loss bucket for high-lift rotor blading of Clark (Ref. 11), showing cruise (design air angles) and take-off (–50° incidence) operation. (a) 2-D mid-span loss bucket. (b) Flow in representative LCTR VSPT rotor at –50° incidence.

Aerodynamic Design Methodology

The conceptual design of the VSPT and the detailed aero design/optimization of airfoil sections and blade rows are documented in this section. The intent of the conceptual design at the meanline level was to obtain flow path geometry, air angles and boundary conditions for subsequent airfoil and 3-D blade row design, and to gauge expected design and off-design performance levels. The intent of the 3-D design was to create a representative embedded 1.5 stage (R1/S2/R2) with design-point stage efficiencies consistent with the meanline, in which the impact of off-design operation of a rotor impacts the off-design performance of a stator (R1/S2), and vice-versa (S2/R2). Stator 1 (S1) was not included in the simulations because the S1 inlet and exit flow angles will not change appreciably with speed change; therefore, the S1 design was assumed achievable, and the S1 exit conditions at design and off-design exit flow conditions were set to those of the meanline analyses.

Conceptual Design/Meanline Analysis

The operational requirements of the VSPT were obtained from NASA engine cycle studies (Ref. 3). Key VSPT requirements were provided in Table 1 for the 2 kft take-off power point (100% N^*) and a 28 kft cruise point (54% N^*).

Design-Point Selection

The VSPT of this study was designed at the 54% N^*, 28 kft cruise condition. As documented earlier (Ref. 4), the following considerations impacted this decision: mission fuel burn is dominated by the 28 kft cruise leg; work factors at cruise are 3 to 3.5 times higher than at take-off, and the associated loss buckets are narrower; the positive-incidence range of the turbine blade rows is 2 to 3 times narrower than the negative-incidence range (see Fig. 2(a)); and, design-point loss-levels increase and the incidence range decrease from take-off to cruise, due to Reynolds number lapse. These factors support the choice to design at cruise, so as to obtain maximum possible efficiency at cruise turbine-speed (54% N^*). The turbine then runs with negative incidence at the higher shaft-speed conditions. As noted, results of meanline and 2-D CFD analyses indicate that the efficiency at the higher shaft-speed points, characterized by lower turning and extreme negative incidence, is predicted to be higher than at the design point.

TABLE 1.—VSPT REQUIREMENTS AT KEY FLIGHT POINTS OF LCTR MISSION (REF. 3)

Flight point	Take-off	Cruise
Altitude	2kft	28 kft
VSPT speed ($N/N_{100\%}$)	100%	54%
Main-rotor tip-speed	650 ft/s	350 ft/s
Power, SHP	4593	2328
VSPT mass flow rate, lb_m/s	22.03	12.22
Specific power (BTU/lb_m)	147	135
PT inlet temp ($T_{4.5}$), R	2204	1812
PT inlet pres. ($p_{0,4.5}$), psia	58.0	26.76
PR_{TT}	4.04	5.34
Corrected flow, lb_m/s	11.51	12.54
Corrected speed ($Nc/Nc_{100\%}$), %	102.3	60.8
Aft-stage unit-Re (in^{-1})[a]	50,000/in.	30,000/in.

[a]Based on static conditions at last stage rotor exit with $M_{r,2} = 0.7$.

Four-Stage Turbine Design at Meanline Level

The turbine flow path, number of stages, and design air angles were determined using F. Huber's meanline design and off-design codes, which are constituents of the AFRL

Turbine Design and Analysis System (TDAAS) (Ref. 11). The meanline codes are consistent with the open-literature methodology of Ainley-Mathieson (Ref. 6), Dunham and Came (Ref. 7), and Kacker and Okapuu (Ref. 8), referred to herein as AMDCKO (see Fig. 1). As in previous work (Ref. 4), the aerodynamic loading levels of the vanes (Z = 1) and blades (Z = 1.1) are set near unity so as to be consistent with operation with transitional flow (Ref. 13) and required incidence-tolerance. The stage reaction levels were set near 0.45. The stage work splits were based on trades between optimum efficiency and management of maximum turning per stage. The rotors were tip-shrouded and leakage flows were neglected. Huber's off-design code (meanline) was used to assess off-design operation. Example design- and off-design point performance levels from the Huber code were provided in Figure 1.

A mechanical design constraint of maximum AN^2 based on temperatures and anticipated material properties was imposed at take-off (100% N^*) hot condition (Ref. 4). In the 4-stage design of the previous study (Ref. 4), the mechanical limit was set at $AN^2 = 45 \cdot 10^9$ rpm^2·in.^{2}, corresponding to an aft blade-row exit annulus area of A_{ex} = 212 in.^{2} and 100% speed of 14,560 rpm. In the 4-stage design considered here, the exit area was maintained at A_{ex} = 212 in.^{2} and 100% shaft speed was increased to 15,000 rpm ($AN^2 = 47.7 \cdot 10^9$ rpm^2·in.^{2}).

The VSPT flow path is provided in Figure 3. Key turbine parameters, including blade row incidence levels at off-design, are provided in Table 2, and the design flow angles are provided in Table 3. Note that design-point blade-row turning levels are as high as 110°.

High negative incidence levels (–40 to –60°) are experienced by all blade rows (blade, vane, and EGV) at off-design operation (see Table 2 and Ref. 4). In spite of the incidence levels at 100% N^*, the VSPT operating map (Fig. 4) reflects the increase in efficiency as speed is changed from the 8,100 rpm (54% N^*) at the cruise design point to the 15,000 rpm (100% N^*) at take-off. Note that the corrected flow in the turbine drops slightly as speed is increased.

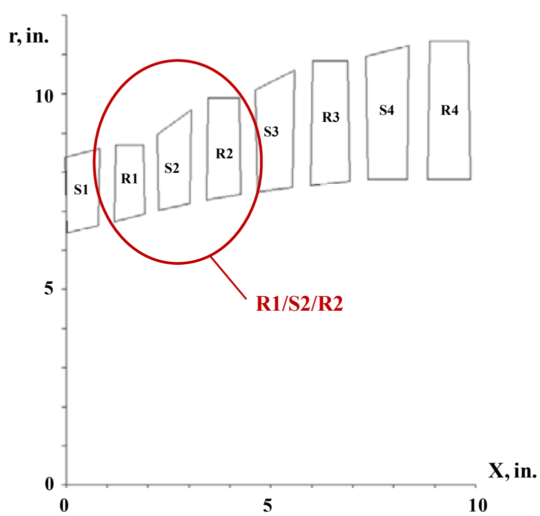

Figure 3.—Four-stage VSPT flow path from Huber's meanline, showing embedded 1.5-stage of computational analysis. No exit guide vane (EGV) shown.

TABLE 2.—FOUR-STAGE DESIGN FOR LCTR VSPT REQUIREMENTS OF TABLE 1

	Take-off	Cruise
Speed ($N/N_{100\%}$)	100%	54%
Altitude, ft	2,000	28,000
VSPT efficiency	0.9294	0.9154
Total-pressure ratio	4.04	5.34
N, rpm	15,000	8,100
Average ψ	0.75	2.36
Average ϕ	0.493	0.957
Average Δh_0, BTU/lb$_m$	41.8	39.1
Max. AN^2, rpm^2·in.^{2}	47.7×10^9	13.9×10^9
Stage efficiency	0.9371, 0.9219, 0.9229, 0.9068	0.9105, 0.8887, 0.9050, 0.9251
Rotor incidence, deg (R1, R2, R3, R4)	–38, –42, –50, –54	0
Stator incidence, deg (S2, S3, S4, EGV)	–34, –40, –48, –35	0
Power, SHP	5287	2701

TABLE 3.—DESIGN-POINT FLOW ANGLES AND LOADING FOR 4-STAGE ROTORS ($AN^2 = 47.7\times10^9$ rpm^2·in.^{2})

Stage	Vane			Rotor		
	α_1	α_2	Turn	β_1	β_2	Turn
1	0	62	62	42	–56	99
2	–39	64	104	50	–60	110
3	–42	62	104	42	–56	98
4	–31	54	85	27	–47	74

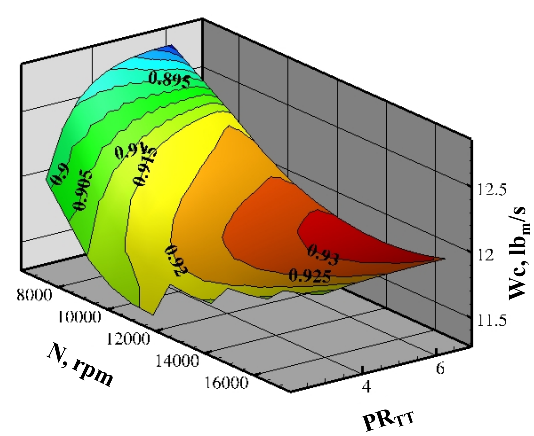

Figure 4.—VSPT performance map in terms of PR_{TT} as a function of corrected flow and rpm of output shaft.

Two-Dimensional Air Foil Design and Stacking

With air angles set in the meanline design (assuming free vortex flow), the TDAAS (Ref. 11) system was used to design and optimize 2-D airfoil sections at hub, mid-span, and tip, and to stack the 2-D sections to construct the 3-D blade geometry. The 2-D sections were generated by Huber's blade profile generator, a 19-parameter description of the turbine blade section, including 5 arbitrary NURBS control points. Within TDAAS, the blade generator is driven by a MATLAB script, and contains options for Design-of-Experiments (DOE) and gradient search optimization. Effort was expended in selecting chordwise loading distributions with minimum pressure placed toward the front to mid-chord regions, consistent with lower-loss operation at low Reynolds numbers (Ref. 13). The 2-D analysis of blade sections was conducted using the commercial software of AeroDynamic Solutions, Inc. (ADS). H-O-H grids were generated about blade sections using the ADS WAND code and fully turbulent κ−ω RANS solutions were obtained using the ADS LEO solver. Design-intent for each blade section included matching meanline geometry, flow angles, gauge angles, and Mach numbers while minimizing total-pressure loss coefficient. The key parameters of the DOE optimization were the blade setting angle, the leading edge wedge angle, and NURBS control points controlling area- and blade-thickness distributions. The hub, mid-span, and tip blade-sections for the R1, S2, and R2 blade rows are shown in Figures 5, 6, and 7.

The hub, mid, and tip sections of a given blade row were stacked on their center of gravity along a radial stacking axis. No dihedral was considered in the present study, although the benefits of using 3-D aerodynamic design—including bow and lean—are well documented for turbines (see, for example, Hourmouziadis (Ref. 14).

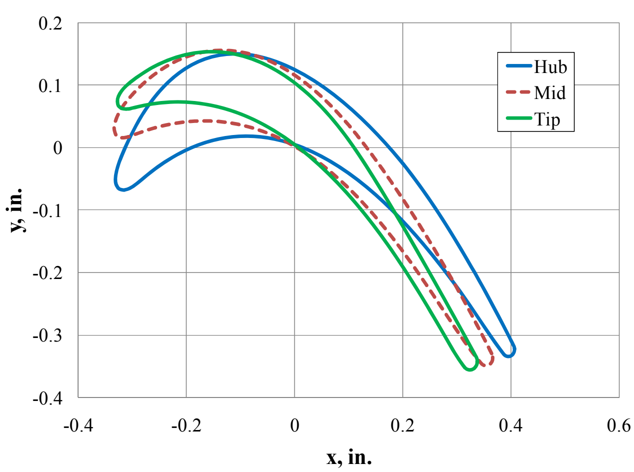

Figure 5.—Hub, mid-, and tip-sections of Rotor 1.

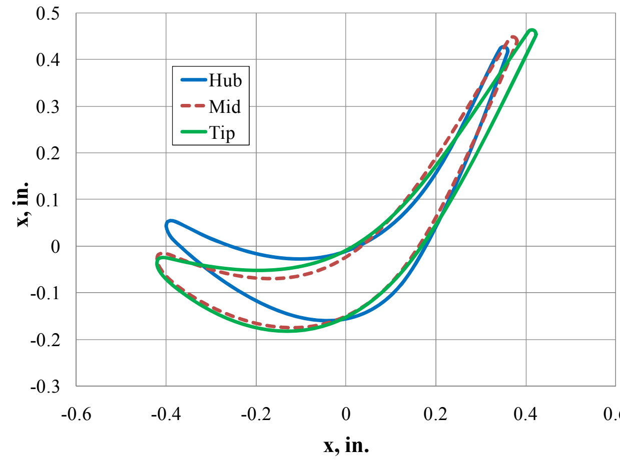

Figure 6.—Hub, mid-, and tip-sections of Stator 2.

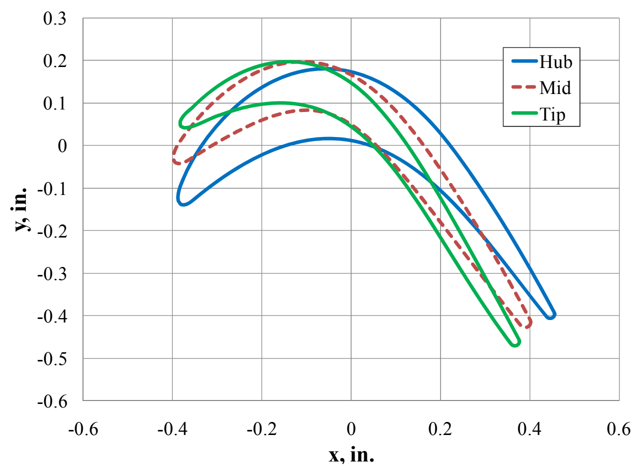

Figure 7.—Hub, mid-, and tip-sections of Rotor 2.

Three-Dimensional CFD Analysis Method

The 3-D blading was analyzed at design and off-design conditions using 3-D RANS turbomachinery flow solver, SWIFT (Ref. 15). The finite-difference form of the thin-layer Navier-Stokes equations in Cartesian coordinates are marched in pseudo-time using a multi-stage explicit Runge-Kutta integration with implicit residual smoothing. Inviscid flux vector differences are calculated using central-difference with artificial viscosity, or with the H-CUSP (used herein) or AUSM$^+$ upwind schemes. The viscous terms are central differenced. Three-dimensional C-grids without clearance blocks were used in all blade rows and were generated using the TCGRID code (Ref. 16). A suite of turbulence sub-models are available, including the Baldwin-Lomax (Ref. 17) (B-L) and low-Re κ−ω turbulence model for transitional flows (Ref. 18) used in this study. The SWIFT code has been validated against a number of turbomachinery data sets.

Boundary conditions were obtained from the design and off-design meanline analyses. Inlet total conditions and swirl angles at the mid-span were prescribed along with an assumption of free-vortex flow. The free vortex flow is consistent with the spanwise flow distributions of the meanline code and the 2-D airfoil design. Radial equilibrium and a specified hub static pressure were prescribed at the exit.

The mixing-plane interface condition was used between blade rows. In addition to neglecting unsteady blade-row interaction, the mixing-plane approach does not conserve streamwise vorticity between blade rows. While these limiting assumptions will impact accuracy, particularly at off-design and high-load conditions, the accuracy was deemed sufficient to address the principal question of the study concerning the trend of VSPT efficiency trend with speed change.

Computational Results

Computational results for the design (54% N^*, 28 kft cruise) and off-design (100% N^*, 2 kft take-off) performance of the embedded 1.5-stage turbine comprising R1, S2, and R2 are considered in this section. First computed design and off-design spanwise profiles are compared to meanline predictions. At both design (54% N^*) and off-design (100% N^*), the 3-D structures associated with secondary flow transport and rotor acceleration fields are discussed. Finally, the blade row, stage, and overall 1.5-stage performance levels at design and off-design are compared.

Design Point (Cruise at 28 kft, 54% N*)

Spanwise Profiles

Spanwise profiles of passage-averaged (mixed-out) normalized total-temperature and total-pressure (referenced to S1 inlet) and absolute flow angles are provided below (Figs. 8 to 10). The computed R1 inlet total-temperature is unity (not plotted in Fig. 8), as specified by the meanline analysis. The computed inlet boundary-layer thickness is evident in the R1 inlet total-pressure profile (black) in Figure 9. The computed R1 inlet absolute flow angle (black) of Figure 10 matches the free-vortex profile of the meanline.

In general, the agreement between the 3-D CFD and meanline for total-temperature (Fig. 8), an indication of work, and total-pressure (Fig. 9) is acceptable, although lower enthalpy extraction is achieved by R2 for the prescribed total-to-static pressure ratio. A large deficit in passage-averaged total-pressure is evident from 60 to 95% of span at the exit of S2; similarly, the hub of the R2 discharge is weak from hub to 20% of span. These low total-pressure sections are consistent with the cross-passage contours of entropy shown Figure 11. In addition to low enthalpy extraction (and associated turning) in R2 for the prescribed total-to-static pressure ratio, the axial rating planes for the CFD and meanline are not coincident, and this may contribute to the disparity in flow angles in Fig. 10.

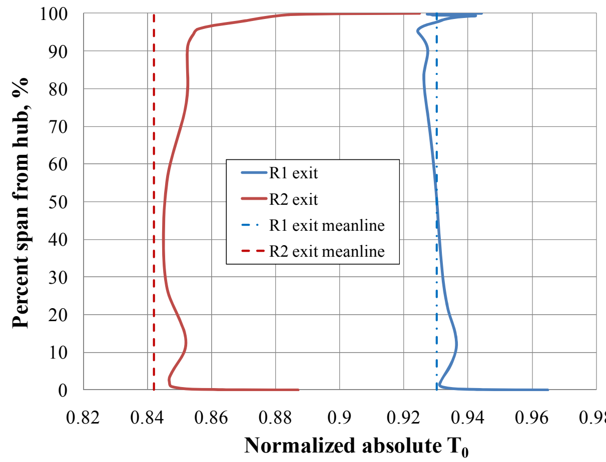

Figure 8.—Spanwise profiles of normalized total-temperature, T_0, at R1 and R2 exits, showing comparison with meanline at design point (54% N^*, 2 kft cruise).

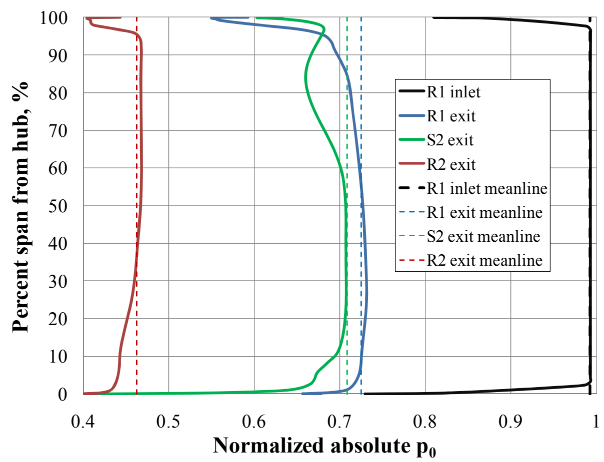

Figure 9.—Spanwise profiles of normalized total-pressure, p_0, at R1 inlet and R1, S2, and R2 exits, showing comparison with meanline at design point (54% N^*, 2 kft cruise).

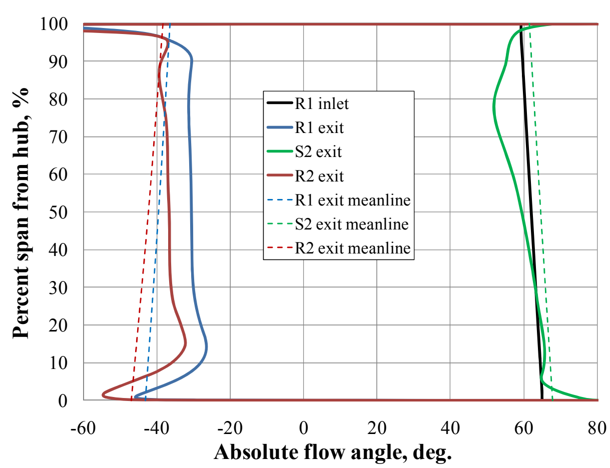

Figure 10.—Spanwise profiles of absolute flow angle at R1 inlet and R1, S2, and R2 exits, showing comparison with meanline at design point (54% N^*, 2 kft cruise).

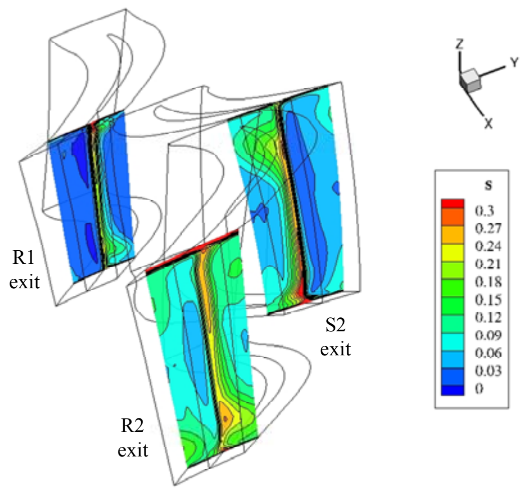

Figure 11.—Computed contours of entropy at the blade-row exit planes at design point.

Three-Dimensional Flow Field

Entropy contours at the exit plane of blade rows R1, S2, and R2 are provided in Figure 11. The low momentum flow, transported by the secondary flow field, accumulates preferentially at the hub/suction-side corners of the rotors and at the case/suction-suction side corner of the stator. In the present study, these regions of low relative total-pressure are mixed-out between blade rows, and are manifested as axisymmetric bands (not shown) of high entropy flow downstream of each mixing plane; in practice the regions of high aero-blockage would be strong sources of spanwise mixing and unsteadiness in the downstream blade row. An unsteady multistage simulation capability would facilitate accurate account of such mechanisms. Three-dimensional blade and endwall features, including bow and lean (Ref. 14) and nonaxisymmetric endwall contouring (Ref. 19), have been demonstrated to be effective in minimizing the secondary-flow-field transport and associated loss and aerodynamic blockage production. This level of aerodynamic design was not pursued in this study.

Off-Design Point (Take-Off at 2 kft, 100% N*)

Spanwise Profiles

Spanwise profiles of normalized total-temperature and total-pressure (referenced to S1 inlet conditions), and absolute flow angle are provided below. R1 inlet plane values of the meanline are plotted where appropriate. As with the design-point, the agreement between the 3-D CFD and meanline for total-temperature (Fig. 12), total-pressure (Fig. 13), and absolute flow angle (Fig. 14) were found acceptable; indeed, the agreement at off-design was perhaps better than at the design point. The computed R2 enthalpy extraction was again low, as at the design point. The aerodynamic loading levels in the blade rows are lower at the higher shaft-speed condition. The total-pressure profiles are more uniform (spanwise) in all sections (Fig. 13). The computed flow turning (Fig. 14) is again found to be low relative to the meanline. This is consistent with lower enthalpy extraction in R2, and may be attributable in part to axial offset of the computational and meanline rating planes.

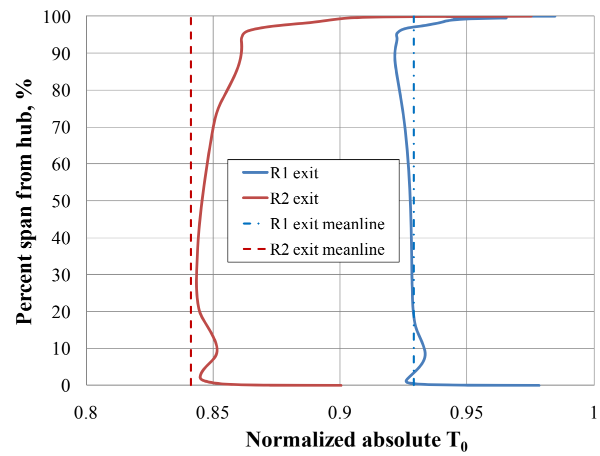

Figure 12.—Spanwise profiles of normalized total-temperature, T_0, at R1 and R2 exits, showing comparison with meanline at off-design (100% N^*, 2 kft take-off).

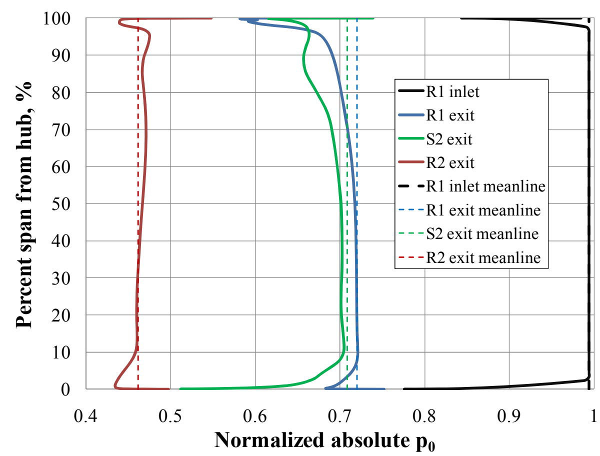

Figure 13.—Spanwise profiles of normalized total-pressure, p_0, at R1 inlet at R1, S2, and R2 exits, showing comparison with meanline at off-design (100% N^*, 2 kft take-off).

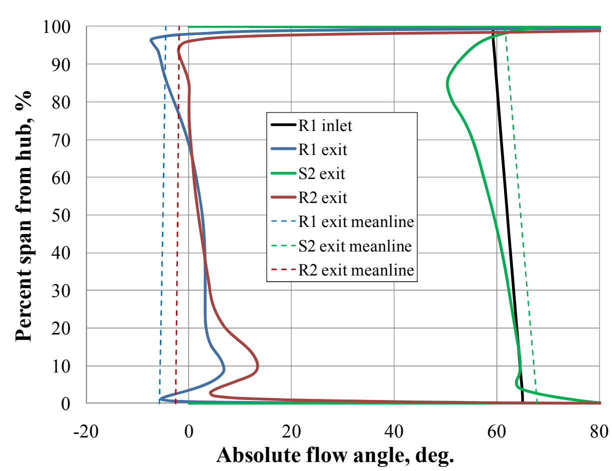

Figure 14.—Spanwise profiles of absolute flow angle at R1 inlet and R1, S2, and R2 exits, showing comparison with meanline at design point (100% N^*, 2 kft take-off).

Three-Dimensional Flow Field

Entropy contours at the exit plane of blade rows R1, S2, and R2 are provided in Figure 15. As at the design point (Fig. 11), the secondary flow fields transport flow to the rotor hub/suction-side corners and stator case/suction-side corner. In general, the regions of lower total-pressure are more diffuse, particularly in the high-turning second rotor, R2, due to radial transport induced by acceleration fields of rotation and associated redistribution of low momentum flow from the hub regions to the casing via the pressure-side cove separation/vortex (Figs. 2(b) and 16).

It was noted that the lower-turning rotor, R1, was not impacted as strongly as the higher turning blade rows (S2 and R2). Indeed a blade-to-blade view of the 1.5-stage (Fig. 16) reflected little reverse flow in the cove region of R1. In R2, a strong vortical structure (tornado) was induced by the radial acceleration fields associated with rotor rotation and the substantial region of reversed flow in the pressure-side cove. Low momentum flow is transported outward, through the cove separation, toward the case. S2 had significant regions of reverse flow in the pressure-side cove as well; however, without the strong radial acceleration fields, no comparable 3-D structure was formed.

Design and Off-Design Performance

The performance of the individual blade rows and overall 1.5-stage were provided in Table 4. The meanline efficiencies reported in Table 4 were re-calculated for this comparison using the temperatures from the meanline and the constant ratio of specific heats of the corresponding 3-D computation. Note, for example, that the S2/R2 efficiency is 0.9005 with this approach rather than 0.8887 (see Table 3) of the meanline output. The CFD parameters are based on mixed-out properties, accounting for loss production in the blade rows and in downstream-mixing.

The computed (B-L and $\kappa-\omega$) R1 rotor-alone efficiencies at design and off-design are consistently about 1 point lower than meanline. The R1 efficiency increases from design to off-design, as in the meanline analysis. The computed stator S2 design-point loss is twice that of the meanline calculation at both design and off-design, and strongly shifts all stage efficiencies to lower levels. The S2 loss decreases from design to off-design in agreement with the meanline. The design- and off-design efficiencies of the high-turning R2 are essentially equal. Relative to the meanline results, R2 efficiency is 2 points low at design and 4.5 points low at off-design. The efficiency variation with speed of the meanline

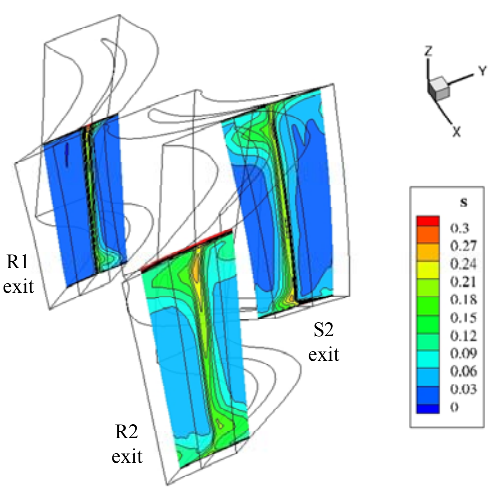

Figure 15.—Computed contours of entropy at the blade-row exit planes at the 100% N* off-design take-off point.

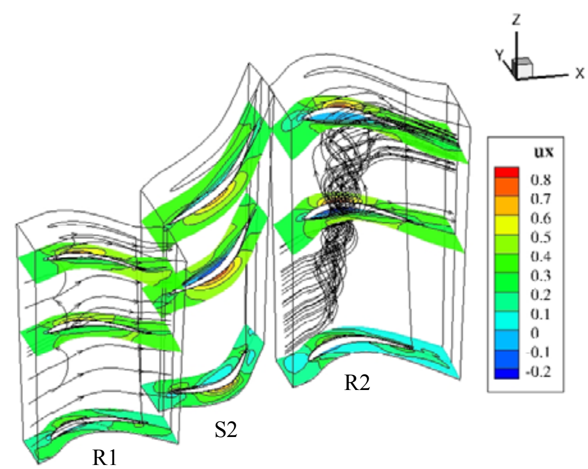

Figure 16.—Computed contours of axial velocity and streamlines in R1 and R2 at the 100% N* off-design take-off point.

TABLE 4.—COMPARISON OF 3-D COMPUTATIONAL RESULTS WITH MEANLINE PREDICTIONS

	Design (54% N*, γ = 1.33)			Off-design (100% N*, γ = 1.315)		
Model	B-L	$\kappa-\omega$[a]	Meanline	B-L	$\kappa-\omega$[a]	Meanline
R1 η_{tt}	0.9108	0.9152	0.9275	0.9439	0.9481	0.9530
R2 η_{tt}	0.9254	0.9329	0.9453	0.9251	0.9258	0.9692
R1/S2 η_{tt}	0.8083	0.8100	0.8682	0.8695	0.8679	0.9080
S2/R2 η_{tt}	0.8398	0.8444	0.9005	0.8334	0.8269	0.9042
R1/S2/R2 η_{tt}	0.8749	0.8792	0.9152	0.9023	0.9013	0.9448
S2 Y	0.1387	0.1414	0.0718	0.1214	0.1326	0.0666
S2 dp0/p0	0.0426	0.0436	0.0222	0.0297	0.0329	0.0165
PR_{TT} R1/S2/R2	2.1438	2.1375	2.1454	2.1303	2.1307	2.1555
TR_{TT} R1/S2/R2	1.1776	1.1779	1.1875	1.1758	1.1756	1.1887
Wc, lb_m/s	12.865	12.942	12.868	12.306	12.423	12.060

[a]Low Reynolds number model.

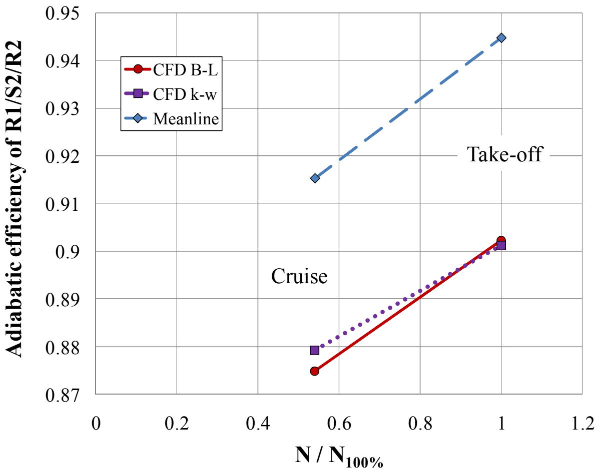

Figure 17.—Variation of embedded 1.5 stage (R1/S2/R2) adiabatic efficiency with speed from cruise (54% N^*) to take-off (100% N^*).

is not supported by the CFD, potentially due to the deleterious impact on performance of the cove vortex (tornado) at the extreme negative incidence of take-off, which is not accounted for in the secondary-flow loss model of the meanline solver.

Embedded Stage Efficiency Trend With Speed Change

The principal objective of the present study was to determine the variation of embedded 1.5-stage (R1/S2/R2) efficiency with speed. As shown in Table 4, the embedded stage efficiency increases from cruise to take-off operation. The variation is plotted in Figure 17. The CFD results were found to follow the meanline. This is the key finding of this study, emphasizing that the design-point shaft-speed should be set near the cruise shaft-speed (54% N^*), as done in the present study.

At both cruise (54% N^*) and take-off (100% N^*), the overall R1/S2/R2 efficiencies predicted by CFD are consistently about four points lower than the meanline values (Fig. 17). The slight change in slope of the low-Re $\kappa-\omega$ model relative to the fully turbulent B-L and meanline models can be attributed to regions of low-loss laminar flow, on the accelerating portions of the suction-side, admitted by the low-Re $\kappa-\omega$ transition sub-model at cruise Reynolds number. Highly loaded aft stages may well trend differently.

Conclusions

The performance of representative blade rows of a variable-speed power turbine for the NASA LCTR application, in particular the variation of efficiency with shaft-speed change, was the subject herein. A conceptual design of the LCTR VSPT led to a 4-stage turbine designed for an altitude (28 kft) cruise point. The turbine performance map and key turbine parameters were provided. The design approach led to a turbine with 91.5% cruise-point (54% N^*, 28 kft) efficiency and 92.9% efficiency at take-off (100% N^*, 2 kft) at the meanline level.

A key objective of the study was to verify, using 3-D RANS analyses, the efficiency versus speed trend of the meanline analyses. The concern was that 3-D flow features associated with transport due to radial acceleration fields and cross-passage gradients would lead to higher losses at the extreme negative incidence operation of the 100% N^* take-off condition than predicted by the meanline loss correlations and 2-D CFD analyses. To this end, a 3-D design of a representative embedded 1.5-stage was designed and analyzed. The design- and off-design performance were found to be sufficiently close to the design intent to be considered relevant for use in assessing the variation of efficiency with shaft-speed.

Two significant 3-D aero effects were noted in the 3-D RANS analyses. Firstly, as normative in highly loaded blade rows, the secondary flow fields transported low momentum fluid to the rotor hub/suction-side corners and stator case/suction-side corners. This occurred at both design and off-design conditions. Secondly, at the 100% N^* off-design condition, the separation in the cove region of the pressure-side of R2 and the radial acceleration fields combined to form a tornado-like structure which transported flow radially outward along the cove to the case. No such structure existed in the first rotor, R1, as the negative incidence levels in the first rotor did not cause a cove separation. Although a strong cove separation was found in S2 at off-design, the absence of the acceleration fields of rotation precluded formation of the tornado-like cove vortex found in R2.

Consistent with meanline analyses, the blade-row loss levels were generally found to be lower at the off-design conditions where, though operating with 40 to 60-deg. of negative incidence, the blade rows are unloaded. An exception to this general trend of higher efficiency at off-design was found in R2, attributable to the impact of the 3-D cove vortex. This finding may push future rotor airfoil designs toward thicker sections that admit less of a pressure-side cove. Enhancement of the meanline secondary loss model for rotors at extreme negative incidence, to account for increased loss due to such 3-D structures, appears to be warranted as well.

Although the regions of loss associated with the 3-D flow structures detailed here reset the spanwise profiles, as shown in the CFD and meanline comparisons, the variation of embedded 1.5-stage efficiency with shaft-speed was found to match that predicted by the meanline. This agreement between 3-D RANS computations and the meanline both corroborates the incidence correlation of the meanline code—with the exception of R2 deficiency noted above—and supports the conceptual design approach that establishes the design speed at the lowest operating shaft speed (54% N^*, cruise). In practice, the specific VSPT design speed is expected to be strongly biased toward the cruise shaft-speed, and selected so as to minimize mission fuel burn.

References

1. Acree, C.W., Hyeonsoo, Y., and Sinsay, J.D., “Performance Optimization of the NASA Large Civil Tiltrotor,” Proc. Int. Powered Lift Conf., London, UK, July 22–24, 2008.
2. Wilkerson, J.B. and Smith, R.L., “Aircraft System Analysis of Technology Benefits to Civil Transport Rotorcraft,” NASA/CR—2009-214594, June, 2009.
3. Snyder, C.A. and Thurman, D.R., "Gas Turbine Characteristics for a Large Civil Tilt-Rotor (LCTR)," *Proc. AHS Int. 65th Ann. Forum*, Grapevine, TX, May, 2009; also NASA/TM—2010–216089, Feb. 2010.
4. Welch, G. E., “Assessment of Aerodynamic Challenges of a Variable-Speed Power Turbine for Large Civil Tilt-Rotor Application,” *Proc. AHS Int. 66th Ann. Forum*, Phoenix, AZ, May, 2010; also NASA/TM—2010-216758, Aug. 2010.
5. D′Angelo, M., “Wide Speed Range Turboshaft Study,” NASA/CR—1995–198380, Aug. 1995.
6. Ainley, D.G. and Mathieson, G.C.R., “A Method of Performance Estimation for Axial-Flow Turbines,” Aeronautical Research Council (ARC), R&M 2974, 1957.
7. Dunham, J. and Came, P.M., “Improvements to the Ainley-Mathieson Method of Turbine Performance Prediction,” *J. Eng. for Power*, July, 1970, pp. 252–256.
8. Kacker S.C., and Okapuu. U., “A Mean Line Prediction Method for Axial Flow Turbine Efficiency,” *J. Eng. Power*, **104**, Jan, 1982, pp. 111–119.
9. Smith, S.F., “A Simple Correlation of Turbine Efficiency,” *J. Royal Aero. Soc*., **69**, 1965, p. 467–470.
10. Oates, G.C, Aerothermodynamics of Aircraft Engine Components, AIAA Education Series, 1985.
11. Clark, J.P., Koch, P.J., Ooten, M.K., Johnson, J.J., Dagg, J., McQuilling, M.W., Huber, F., and Johnson, P.D., “Design of Turbine Components to Answer Research Questions in Unsteady Aerodynamics and Heat Transfer,” AFRL-RZ-WP-TR-2009-2180, Sept, 2009.
12. Ainley, D.G. and Mathieson, G.C.R., “An Examination of Flow and Pressure Losses in Blade Rows of Axial Turbines, British Aeronautical Research Council (ARC), R&M 2891, 1955.
13. Gier, J., Franke, M., Hübner, N. and Shröder, T., “Designing LP Turbines for Optimized Airfoil Lift,” *J. Turbomachinery*, **132**, Jul, 2010, pp. 031008-1 to -12.
14. Hourmouziadis, J., “Aerodynamic Design of Low Pressure Turbines,” in *Blading Design for Axial Turbo-machines*, AGARD-LS-167, pp. 8–1 to 8–40, 1989.
15. Chima, R.V., "Calculation of Multistage Turbomachinery Using Steady Characteristic Boundary Conditions," AIAA-98-0968, Jan. 1998; also NASA/TM—1998-206613.
16. Chima, R.V., “TCGRID 3-D Grid Generator for Turbomachinery—User’s Manual and Documentation,” Dec. 1999.
17. Baldwin, B.S. and Lomax, H., “Thin-Layer Approximation and Algebraic Model for Separated Turbulent Flows,” AIAA 78–257, Jan. 1978.
18. Wilcox, D.C., *Turbulence Modeling for CFD,* DCW Industries, Inc., La Canada, CA, 1994.
19. Knezevici, D.C., Sjolander, S.A., Praisner, T.J., AllenBradley, E., Grover, E.A., “Measurements of Secondary Losses in a Turbine Cascade With the Implementation of Nonaxisymmetric Endwall Contouring,” *J. Turbomachinery*, **132**, Jan, 2010, pp. 011013-1 to -10.

REPORT DOCUMENTATION PAGE				*Form Approved* *OMB No. 0704-0188*

1. REPORT DATE *(DD-MM-YYYY)*
01-11-2011

2. REPORT TYPE
Technical Memorandum

3. DATES COVERED *(From - To)*

4. TITLE AND SUBTITLE
Computational Assessment of the Aerodynamic Performance of a Variable-Speed Power Turbine for Large Civil Tilt-Rotor Application

5a. CONTRACT NUMBER

5b. GRANT NUMBER

5c. PROGRAM ELEMENT NUMBER

6. AUTHOR(S)
Welch, Gerard, E.

5d. PROJECT NUMBER

5e. TASK NUMBER

5f. WORK UNIT NUMBER
WBS 877868.02.07.03.01.02.01

7. PERFORMING ORGANIZATION NAME(S) AND ADDRESS(ES)
National Aeronautics and Space Administration
John H. Glenn Research Center at Lewis Field
Cleveland, Ohio 44135-3191

8. PERFORMING ORGANIZATION REPORT NUMBER
E-17813

9. SPONSORING/MONITORING AGENCY NAME(S) AND ADDRESS(ES)
National Aeronautics and Space Administration
Washington, DC 20546-0001

10. SPONSORING/MONITOR'S ACRONYM(S)
NASA

11. SPONSORING/MONITORING REPORT NUMBER
NASA/TM-2011-217124

12. DISTRIBUTION/AVAILABILITY STATEMENT
Unclassified-Unlimited
Subject Category: 07
Available electronically at http://www.sti.nasa.gov
This publication is available from the NASA Center for AeroSpace Information, 443-757-5802

13. SUPPLEMENTARY NOTES

14. ABSTRACT
The main rotors of the NASA Large Civil Tilt-Rotor notional vehicle operate over a wide speed-range, from 100% at take-off to 54% at cruise. The variable-speed power turbine offers one approach by which to effect this speed variation. Key aero-challenges include high work factors at cruise and wide (40 to 60°) incidence variations in blade and vane rows over the speed range. The turbine design approach must optimize cruise efficiency and minimize off-design penalties at take-off. The accuracy of the off-design incidence loss model is therefore critical to the turbine design. In this effort, 3-D computational analyses are used to assess the variation of turbine efficiency with speed change. The conceptual design of a 4-stage variable-speed power turbine for the Large Civil Tilt-Rotor application is first established at the meanline level. The design of 2-D airfoil sections and resulting 3-D blade and vane rows is documented. Three-dimensional Reynolds Averaged Navier-Stokes computations are used to assess the design and off-design performance of an embedded 1.5-stage portion-Rotor 1, Stator 2, and Rotor 2-of the turbine. The 3-D computational results yield the same efficiency versus speed trends predicted by meanline analyses, supporting the design choice to execute the turbine design at the cruise operating speed.

15. SUBJECT TERMS
Low pressure turbine; Rotary wing; Aerodynamics

16. SECURITY CLASSIFICATION OF:			**17. LIMITATION OF ABSTRACT**	**18. NUMBER OF PAGES**	**19a. NAME OF RESPONSIBLE PERSON**
a. REPORT	**b. ABSTRACT**	**c. THIS PAGE**			STI Help Desk (email:help@sti.nasa.gov)
U	U	U	UU	16	**19b. TELEPHONE NUMBER** *(include area code)* 443-757-5802